Magnetic properties of diluted hexaferrites

Logan Sowadski,[1] Sean Anderson,[1] Cameron Lerch,[2] Julia Medvedeva,[1] and Thomas Vojta[1]
[1]*Department of Physics, Missouri University of Science and Technology, Rolla, MO 65409, USA*
[2]*Department of Mechanical Engineering and Materials Science, Yale University, New Haven, Connecticut 06520, USA*
(Dated: November 8, 2022)

We revisit the magnetic properties of the hexagonal ferrite $PbFe_{12-x}Ga_xO_{19}$. Recent experiments have reported puzzling dependencies of the ordering temperature and the saturation magnetization on the Ga concentration x. To explain these observations, we perform large-scale Monte Carlo simulations, focusing on the effects of an unequal distribution of the Ga impurities over the five distinct Fe sublattices. Ab-initio density-functional calculations predict that the Ga ions preferably occupy the 12k sublattice and (to a lesser extent) the 2a sublattice. We incorporate this insight into a nonuniform model of the Ga distribution. Monte Carlo simulations using this model lead to an excellent agreement between the theoretical and experimental values of the ordering temperature and saturation magnetization, indicating that the unequal distribution of the Ga impurities is the main reason for the unusual magnetic properties of $PbFe_{12-x}Ga_xO_{19}$. We also compute the temperature and concentration dependencies of the sublattice magnetizations, and we study the character of the zero-temperature transition that takes place when the ordering temperature is tuned to zero.

I. INTRODUCTION

Recent years have seen renewed interest in the properties of hexagonal ferrites (hexaferrites). These materials have numerous technological applications including permanent magnets, magnetic recording and data storage devices, as well as high-frequency electronics [1, 2]. In addition, they feature interesting magnetic and ferroelectric quantum behavior at low temperatures [3–5].

The magnetic properties of hexaferrites can be tuned by diluting the magnetic degrees of freedom. Several experimental studies [5–7] reported the results of randomly substituting nonmagnetic Ga ions for the magnetic Fe ions in magnetoplumbite, $PbFe_{12}O_{19}$. Magnetoplumbite is a Lieb-Mattis type ferrimagnet [8] with a magnetic ordering temperature T_c of about 720 K and a low-temperature saturation magnetization M_s of $20\mu_B$ per formula unit. The magnetic ordering temperature of $PbFe_{12-x}Ga_xO_{19}$ decreases with increasing Ga concentration x and vanishes at a critical concentration $x_c \approx 8.6$. The value of x_c is very close to the site percolation threshold of the lattice spanned by the exchange interactions between the Fe ions, suggesting that the zero-temperature magnetic phase transition at x_c is of percolation type [5]. The magnetic phase boundary can be approximated well by the relation $T_c(x) = T_c(0)(1 - x/x_c)^\phi$ with $\phi = 2/3$ over the entire concentration range. Interestingly, the low-temperature saturation magnetization M_s decreases much faster with x than T_c, as is shown in Fig. 1.

To explain these findings, Khairnar et al. [9] performed Monte Carlo simulations of a randomly diluted Heisenberg model, employing the magnetoplumbite crystal structure and realistic exchange interactions. As shown in Fig. 1, the results of these simulations did not agree with the experimental data. Specifically, the ordering temperature predicted by the simulations is *lower* than the experimental values and does not follow the striking 2/3 power law, whereas the saturation magnetization predicted by the simulations is significantly *higher* than the experimental findings. This is a puzzling situation for at least two reasons. First, while it is relatively easy to identify possible mechanisms that could lead to a faster reduction of T_c with x compared to a simple Heisenberg Hamiltonian (e.g., frustrating interactions, non-collinear order, or quantum fluctuations) it is harder to find reasons for the experimental T_c to de-

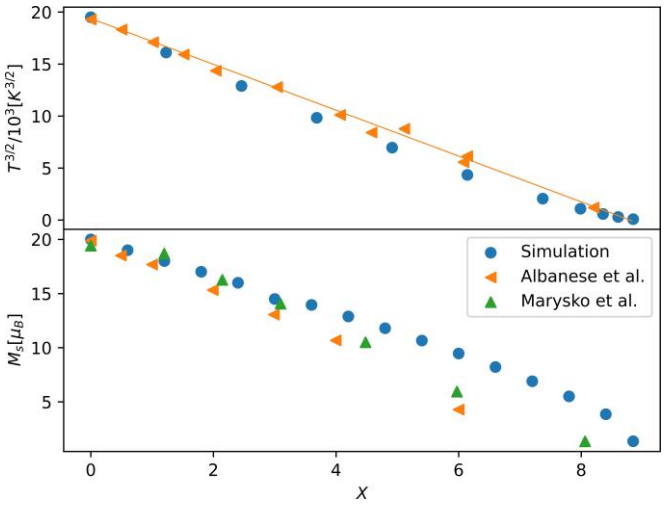

FIG. 1. Magnetic ordering temperature T_c (top) and low-temperature saturation magnetization M_s per formula unit (bottom) of $PbFe_{12-x}Ga_xO_{19}$ as functions of the Ga concentration x. The experimental data for T_c are taken from Refs. [5, 7], and the M_s data stem from Refs. [6, 7]. The solid line represents the 2/3-power law for T_c put forward in Ref. [5]. The Monte Carlo simulations assumed a uniform distribution of the Ga atoms over all available iron sites. The results for T_c are from Ref. [9] whereas those for M_s were computed here, using the algorithm of Ref. [9].

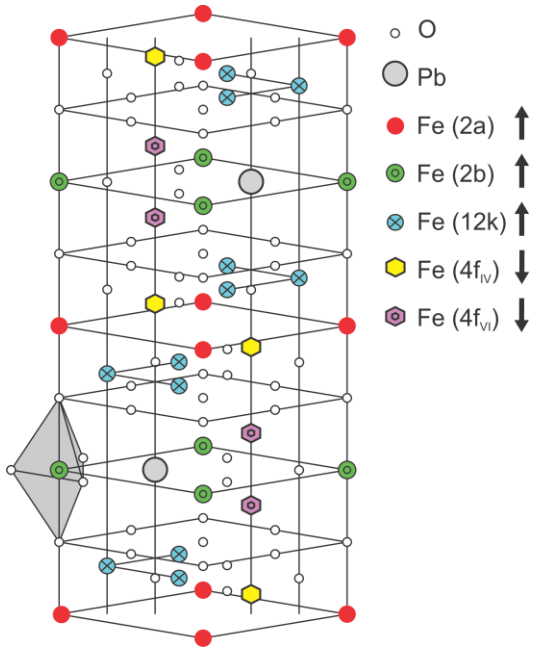

FIG. 2. Double unit cell of $PbFe_{12}O_{19}$. Twelve Fe^{3+} ions per unit cell are located on five distinct sublattices.

cay more slowly than the model calculation. Second, one would usually assume that a mechanism that increases T_c to also increase M_s, but the experimental M_s values are below the simulation results. In summary, these finding imply that our understanding of the magnetic properties of the diluted hexaferrites remains incomplete, especially at higher dilutions.

The M -type hexaferrites $PbFe_{12}O_{19}$, $BaFe_{12}O_{19}$ and $SrFe_{12}O_{19}$ crystalize in the magnetoplumbite structure presented in Fig. 2. The twelve Fe^{3+} ions per unit cell, each in the S=5/2 spin state, are located on five distinct sublattices: 6 ions on the octahedral 12k sublattice, one ion on the octahedral 2a sublattice, one ion on the pseudohexahedral 2b sublattice, two ions on the tetrahedral 4f_{IV} sublattice, and two ions on the octahedral 4f_{VI} sublattice. Below T_c of about 720 K, the spins feature collinear ferrimagnetic order with eight spins (12k, 2a, and 2b) pointing up and four spins (4f_{IV} and 4f_{VI}) pointing down.

As the crystal structure contains five inequivalent iron sublattices, the distribution of the gallium ions over these sublattices can be expected to play an important role for the magnetic properties. In fact, this question has been considered in several publications in the literature, with inconclusive results. Marysko et al. [6] concluded from their magnetic measurements and ferromagnetic resonance experiments that the Ga^{3+} ions are distributed over all sublattices except the 2b sublattice, at least for x up to about 4 (in analogy with earlier results for other hexaferrites [10, 11]). In contrast, Albanese et al. [7] more recently reported accurate Mössbauer measurements indicating that the Ga^{3+} ions are distributed over all five sublattices with nearly equal probability (even though a slightly higher gallium concentration in the spin-up sublattices could not be excluded). For the related compound $SrFe_{12-x}Ga_xO_{19}$ (whose $T_c(x)$ curve is virtually indistinguishable from that of $PbFe_{12-x}Ga_xO_{19}$ [7]), Mössbauer studies [12] suggested that the Ga ions preferably occupy the octahedral 4f_{VI} site. First-principle calculations [13], in contrast, show a strong preference of the Ga ions for the 12k sublattice.

The percolation calculations in Ref. [5] as well as the Monte Carlo simulations of Ref. [9] were performed under the assumption that the Ga impurities are distributed with equal probability over all sublattices. In view of the disagreement between the magnetic measurements on $PbFe_{12-x}Ga_xO_{19}$ and the results of the Monte Carlo simulations in the literature, it is prudent to revisit this assumption.

In the present paper, we therefore combine ab-initio density functional calculations and large-scale Monte Carlo simulations to systematically study how an unequal gallium distribution over the available sublattices affects the magnetic properties of $PbFe_{12-x}Ga_xO_{19}$. Our results can be summarized as follows. According to the density functional calculations, the 12k sublattice is the most favorable location for the Ga^{3+} ions, followed by the 2a sublattice. Ga^{3+} ions in any of the other sublattices lead to significantly higher total energies. We use this insight to construct a diluted Heisenberg Hamiltonian with a biased distribution of spinless impurities. Monte Carlo simulations of this Hamiltonian lead to an excellent agreement between the experimental data for the ordering temperature T_c and the low-temperature saturation magnetization M_s and the corresponding simulation results. This indicates that the unequal distribution of gallium impurities is the main reason for the unusual magnetic behavior of $PbFe_{12-x}Ga_xO_{19}$.

The rest of the paper is organized as follows. In Sec. II, we introduce the site-diluted Heisenberg Hamiltonian, and we discuss the density functional calculations that inform our model of the impurity distribution. The Monte Carlo simulation methods and data analysis techniques are described in Sec. III. Section IV is devoted to the simulation results and the comparison with the experimental data. We conclude in Sec. V.

II. MODEL

A. Site-diluted Heisenberg Hamiltonian

The high spin value $S = 5/2$ of the Fe^{3+} ions and the high ordering temperature of about 720 K for the undiluted compound suggest that a classical approach to the magnetic degrees of freedom should provide a good approximation. To describe the magnetism of $PbFe_{12-x}Ga_xO_{19}$, we therefore define a classical Heisenberg model by placing either a classical Heisenberg spin or a vacancy on each Fe site in the hexaferrite crystal

sublattice pair	$2a-4f_{\rm IV}$	$2b-4f_{\rm VI}$	$12k-4f_{\rm IV}$	$12k-4f_{\rm VI}$
K_{ij}	5 meV	5 meV	3.5 meV	5 meV
J_{ij}	439 K	439 K	311 K	439 K

TABLE I. Values of the exchange interactions. K_{ij} denotes the interactions computed in Ref. [15] for $U_{\rm eff}$ = 6.7. We have absorbed the values of the magnetic moments into the interactions J_{ij} used in the Heisenberg Hamiltonian (1) and scaled them with a constant factor c = 1.212 to reproduce the clean ordering temperature of 720 K, i.e., $J_{ij} = (5/2)^2 c K_{ij}$

structure. The Hamiltonian is given by

$$H = \sum_{i,j} J_{ij}\epsilon_i\epsilon_j \, \mathbf{S}_i\mathbf{S}_j \ . \qquad (1)$$

Here, $\mathbf{S}_i$ is an $O(3)$ unit vector at site i. The exchange interactions J_{ij} are all positive, i.e., antiferromagnetic. We base their values on density functional calculations in Refs. [14, 15] (for $BaFe_{12}O_{19}$) and Ref. [16] (for $SrFe_{12}O_{19}$). The resulting interactions depend weakly on the value of $U_{\rm eff}$ assumed in the density functional algorithm, and they vary somewhat between the different calculations. However, scaling the interactions by a common factor to reproduce the clean ordering temperature $T_c = 720K$ of the undiluted material suppresses most of these variations. In our simulations, we only include the strongest interactions which are between the following sublattice pairs: $2a-4f_{\rm IV}$, $2b-4f_{\rm VI}$, $12k-4f_{\rm IV}$, $12k-4f_{\rm VI}$. Their values are listed in Table I. These interactions are non-frustrated and establish the ferrimagnetic order. We will discuss in the concluding section the effects of additional couplings which are significantly weaker but frustrate the ferrimagnetic order. We employ the exchange interactions computed for the undiluted system for our simulations in entire x-range. This neglects variations of the interactions caused by changes in the lattice geometry due the substitution of Fe ions by Ga ions. These changes are expected to be small because of the small difference between the ionic radii of Ga^{3+} (0.62 Å) and Fe^{3+} (0.64 Å) cations [17].

The ϵ_i are independent quenched random variables that implement the site dilution. The can take the values 0 (vacancy) with probability p_i and 1 (occupied site) with probability $1-p_i$. In the simulations performed in Ref. [9], all lattice sites were assumed to feature the same vacancy probabilities, $p_i = p$ which is related to the average number of Ga ions in the unit cell via $p = x/12$. The goal of the present paper is to explore the effects of deviations from such a uniform Ga distribution. Nonuniform Ga distributions are discussed in detail in the next subsection.

B. Distribution of the Ga impurities

As pointed out in Sec. I, the available results on the distributions of the Ga ions over the five Fe sublattices [6, 7] are inconclusive and partially contradict each other. We have therefore performed ab-initio density functional calculations which suggest a non-uniform Ga distribution which has a strong bias towards the 12k sublattice and smaller bias towards the 2a sublattice.

To model a nonuniform vacancy distribution in the Heisenberg Hamiltonian (1), we introduce weights $w(2a)$, $w(2b)$, $w(4f_{\rm IV})$, $w(4f_{\rm VI})$, and $w(12k)$ that modify the vacancy probability compared to the uniform case. Specifically, the vacancy probability in sublattice Y is given by $w(Y)\,p$. Note that the weights have to fulfill the constraint

$$w(2a)+w(2b)+2w(4f_{\rm IV})+2w(4f_{\rm VI})+6w(12k) = 12 \qquad (2)$$

to ensure that the overall vacancy probability in the system still equals p. The uniform case is recovered if all weights are equal to unity.

Motivated by the density functional results, we focus on model distributions where $w(12k)$ is larger than unity while all other weights are identical to each other and smaller than unity,

$$w(2a) = w(2b) = w(4f_{\rm IV}) = w(4f_{\rm VI}) = 2-w(12k) \ , \qquad (3)$$

fulfilling the constraint (2). We also perform a few exploratory calculations for models in which both $w(12k)$ and $w(2a)$ are increased while all others weights are identical and decreased compared to unity.

III. MONTE CARLO SIMULATIONS

A. Algorithm

We carry out large-scale Monte Carlo simulations of the classical Heisenberg model (1) to determine the magnetic ordering temperature T_c, the saturation magnetization M_s, and other magnetic quantities. These simulations utilize both Wolff cluster updates [18] which are beneficial in reducing critical slowing down of the system near criticality and Metropolis single-spin updates [19] which help equilibrating small isolated clusters of spins which may form due to the site dilution. In our simulations, a full Monte Carlo sweep consists of a Wolff sweep followed by a Metropolis sweep.

We simulate systems consisting of L^3 double unit cells with L ranging from 6 to 48. As each double unit cell contains 24 Fe sites, our largest systems contain about 2.6 million spins. All physical quantities of interest are averaged over 6400 to 25,600 independent disorder configurations for each size. Statistical errors are obtained from the variations of the results between the configurations.

To find the number of Monte Carlo sweeps required for the system to equilibrate, we compare the results of runs

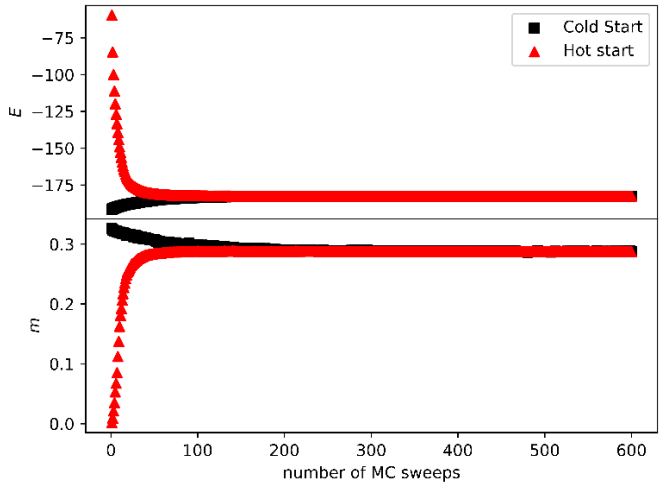

FIG. 3. Equilibration of the energy per site E and the order parameter m for a system of 48^3 double unit cells, dilution $p = 0.66$, weight $w(12k) = 1.25$ and temperature $T = 27$ K . The comparison of hot and cold starts shows that the system equilibrates after roughly 500 Monte Carlo sweeps despite being close to the critical point.

with hot starts (for which the spins initially point in random directions) and with cold starts (for which all spins are initially aligned with the ferrimagnetic order). An example of such a test for a system close to its critical point is shown in Fig. 3. The energy and order parameter reach their equilibrium values after roughly 500 Monte Carlo sweeps. Similar numerical checks were performed for other parameter values. Based on these tests, we have chosen to perform 1000 equilibration sweeps and 2000 measurement sweeps. Note that performing comparatively short Monte Carlo runs for a large number of disorder configurations reduces the total statistical error [20–22].

B. Data analysis

The order parameter $\boldsymbol{\psi}$ of the ferrimagnetic transition in the hexaferrites is the "staggered" magnetization that counts the spin-up sublattices positive and the spin-down sublattices negative,

$$\boldsymbol{\psi} = \frac{1}{N} \sum_i f_i \epsilon_i \mathbf{S}_i \tag{4}$$

where N is the total number of lattices sites. $f_i = 1$ for sites in the $2a$, $2b$, and $12k$ sublattices whereas $f_i = -1$ for the $4f_{IV}$ and $4f_{VI}$ sublattices. In contrast, the physical magnetization is given by

$$\mathbf{m} = \frac{1}{N} \sum_i \epsilon_i \mathbf{S}_i. \tag{5}$$

For easier comparison with experiment, we will use $\mathbf{M} = 20\mu_B \mathbf{m}$, which specifies the magnetization in Bohr magnetons per formula unit. We also compute the sublattice magnetizations $\mathbf{m}_l$ for each of the five Fe sublattices. They are defined as

$$\mathbf{m}_l = \frac{1}{N_l} \sum_{i \in l} \epsilon_i \mathbf{S}_i \tag{6}$$

where the sum runs over all sites in the sublattice, and N_l is their number.

To determine the ordering temperature T_c, we analyze the Binder cumulant [23] of the order parameter. It is defined as

$$g = 1 - \frac{\langle |\boldsymbol{\psi}|^4 \rangle}{3\langle |\boldsymbol{\psi}|^2 \rangle^2}_{dis} . \tag{7}$$

Here $\langle \ldots \rangle$ denotes the thermodynamic (Monte Carlo) average and $[\ldots]_{dis}$ denotes the average over disorder configurations. Because the Binder cumulant g is a dimensionless quantity, it fulfills the finite-size scaling form

$$g(t, L, u) = g(t\lambda^{-1/\nu}, L\lambda, u\lambda^{\delta}) . \tag{8}$$

Here, λ is an arbitrary length scale factor, $t = (T - T_c)/T_c$ is the reduced temperature, and ν is the correlation length critical exponent of the magnetic phase transition. As we anticipate corrections to scaling to be important in the presence of disorder, we have included the irrelevant variable u and the corresponding exponent $\delta > 0$. By setting the scale factor $\lambda = L^{-1}$, we obtain $g(t, L, u) = F(tL^{1/\nu}, uL^{-\delta})$ where F is a dimensionless scaling function. Expanding F in its second argument results in

$$g(t, L, u) = \Phi(tL^{\frac{1}{\nu}}) + uL^{-\delta}\Phi_u(tL^{\frac{1}{\nu}}) . \tag{9}$$

If corrections to scaling are negligible ($u = 0$), the Binder cumulant curves for different system sizes all cross at the universal value $\Phi(0)$. If corrections to scaling cannot be neglected ($u \neq 0$), this is not the case. Instead, the crossing point shifts with L and approaches $t = 0$ as $L \to \infty$. Expanding the scaling functions Φ and Φ_u gives the following expression for the crossing temperature $T^*(L)$ between the Binder cumulant curves for sizes L and cL (where c is a constant):

$$T^*(L) = T_c + bL^{-\omega} \quad \text{with} \quad \omega = \delta + \frac{1}{\nu} \tag{10}$$

where $b \sim u$ is a non-universal amplitude [9]. This system size dependence can be used to extrapolate the numerically found crossing temperatures to infinite system size, as is illustrated in Fig. 4.

IV. RESULTS

A. Critical Ga concentration from percolation theory

Before we turn to the Monte Carlo simulations, we determine the critical Ga concentration, i.e., the Ga concentration at which the ordering temperature is suppressed

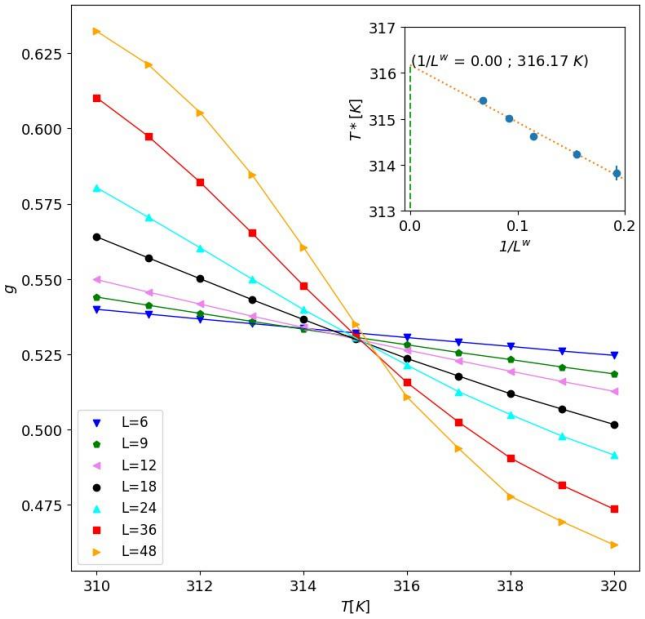

FIG. 4. Binder cumulant g vs. temperature T for several system sizes L, dilution $p = 0.5$ and weights $w(12k) = 1.25$, $w(2a) = w(2b) = w(4f_{\mathrm{IV}}) = w(4f_{\mathrm{VI}}) = 0.75$. The statistical errors are smaller than the symbol size. Inset: Extrapolation of the crossing temperature T^* to infinite system size, using the exponent value $w = 1.5$.

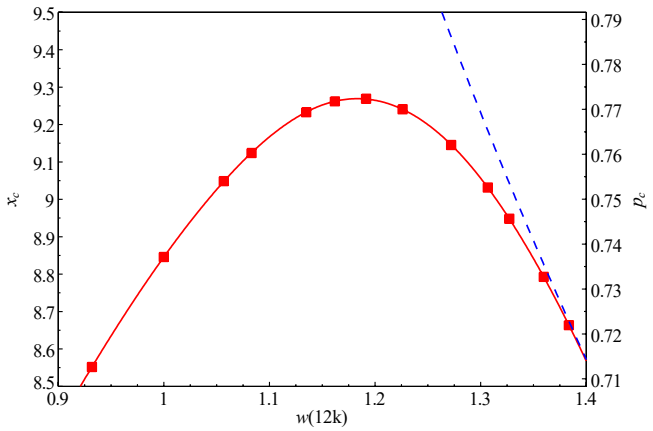

FIG. 5. Critical Ga concentration x_c and the corresponding critical vacancy probability $p_c = x_c/12$ as functions of the weight $w(12k)$. The statistical errors of the data points are much smaller than the symbol size. The solid line is a guide to the eye only. The dashed line represents the Ga concentration $x = 12/w(12k)$ at which the $12k$ sublattice becomes completely depleted of Fe atoms.

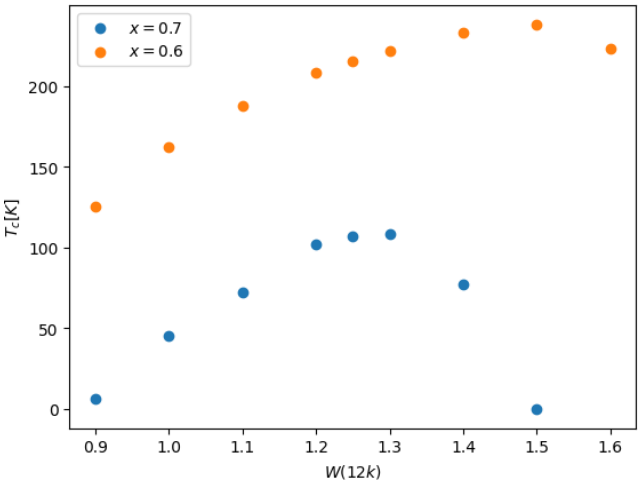

FIG. 6. Magnetic ordering temperature T_c as a function of the weight $w(12k)$ at fixed Ga concentrations $x = 0.6$ and 0.7. The statistical errors are smaller than the symbol size.

to zero, by means of percolation theory. Specifically, we compute the site percolation threshold of the lattice spanned by the nonfrustrated interactions listed in Table I, taking into account that the vacancy probability varies from sublattice to sublattice.

We employ a version of the fast percolation algorithm by Newman and Ziff [24] which allows us to study systems of up to 300^3 double unit cells (648 million Fe sites). For each system size, the percolation threshold is determined from the onset of a spanning cluster, averaged over several hundred disorder configurations. The results are then extrapolated to infinite system size.

We have applied this analysis to a sequence of systems with varying vacancy weight $w(12k)$ for the $12k$ sublattice. All other sublattices have identical weights given by Eq. (3). Figure 5 presents the resulting critical Ga concentrations. For $w(12k) = 1$, this calculation reproduces the value $x_c = 8.846$ found in Ref. [5]. As $w(12k)$ is increased above unity, the critical Ga concentration first increases. It reaches a maximum of about 9.27 for $w(12k) \approx 1.18$ before decreasing again. For weights $w(12k) \gtrsim 1.4$, the critical Ga concentration is given by $x = 12/w(12k)$ in very good approximation, indicating that the transition coincides with the complete depletion of the $12k$ sublattice. It is worth emphasizing that x_c deviates by less than 5% from its value for a uniform Ga distribution over a wide range of $w(12k)$ between about 0.9 and 1.4.

B. Magnetic phase boundary

We now turn to the results of the Monte Carlo simulations. We start by analyzing how the magnetic ordering temperature T_c depends on the vacancy weights w at fixed overall vacancy concentration. Figure 6 presents T_c vs. $w(12k)$ at fixed $x = 0.6$ and 0.7 for the same sequence of systems as in Fig. 5, i.e. a sequence for which the weight $w(12k)$ differs from all the other weights which are given by Eq. (3). The figure shows that the behavior of T_c is qualitatively similar to that of the critical Ga concentration x_c discussed in Sec. IV A. As the weight

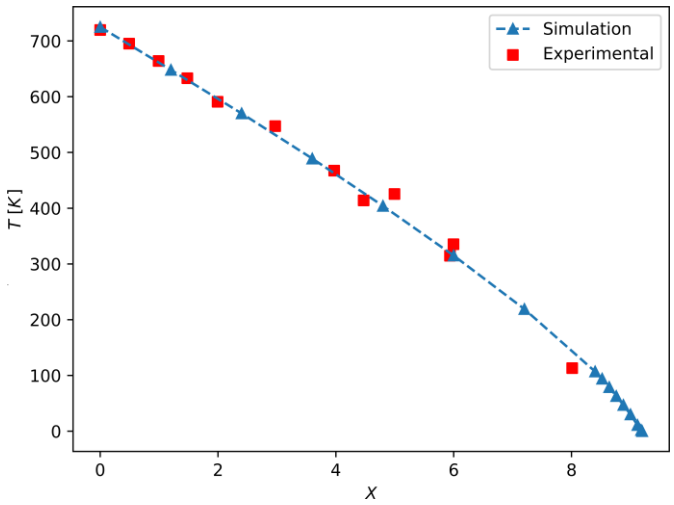

FIG. 7. Magnetic ordering temperature T_c vs. Ga concentration x for $w(12k) = 1.25$. All other weights take the value $2 - w(12k)$. The statistical errors are smaller than the symbol size. The dashed line is a guide to the eye only. The experimental values stem from Refs. [5, 7].

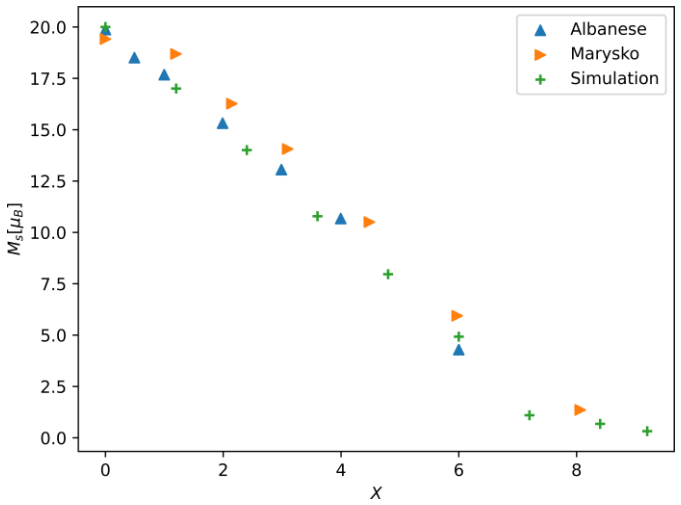

FIG. 8. Low-temperature saturation magnetization M (in μ_B per formula unit) vs. Ga concentration x. for $w(12k) = 1.25$. All other weights take the value $2-w(12k)$. The experimental values stem from Refs. [6, 7].

$w(12k)$ is increased from the uniform case, $w(12k) = 1$, the ordering temperature increases, reaches a maximum, and then decreases for larger $w(12k)$. However, the relative change of T_c is much stronger than that of x_c. The maximum T_c is about 50% higher than the T_c value in the uniform case for $x = 0.6$ and twice as high for $x = 0.7$. Moreover, for weights $w(12k)$ in the range from 1.2 to 1.3, the ordering temperature roughly agrees with the experimental value obtained from the data in Refs. [5, 7] (see Fig. 1).

Based on this observation, we have computed the ordering temperature $T_c(x)$ over the entire x-range between 0 and x_c for the weight $w(12k) = 1.25$. The resulting phase boundary for $w(12k) = 1.25$ is shown in Fig. 7 together with the corresponding experimental data. Clearly, the Monte Carlo results for $w(12k) = 1.25$ are in excellent agreement with experiment, in contrast to the Monte Carlo results for the uniform case, $w(12k) = 1$ shown in Fig. 1. The corresponding $T_c(x)$ curves for weights $w(12k) = 1.2$ and 1.3 deviate only slightly from the phase boundary for $w(12k) = 1.25$.

For comparison, we have also analyzed a case in which the impurity weights in both the $12k$ sublattice and the $2a$ sublattice are increased, $w(12k) = w(2a) = 1.2$, whereas the other weights are reduced, $w(2b) = w(4f_{IV}) = w(4f_{VI}) = 0.72$. The resulting phase boundary is virtually indistinguishable from that for the case (3) with $w(12k) = 1.2$.

C. Saturation magnetization

In addition to the ordering temperature, we have also calculated the low-temperature limit of the magnetization **M**. As all interactions in our model Hamiltonian are nonfrustrated, this value can be directly compared to the low-temperature saturation magnetization M_s measured in experiment. Figure 8 presents M_s vs. x for $w(12k) = 1.2$ and 1.25 [and all other weights given by Eq. (3)] together with the experimental values from Refs. [6, 7]. The figure demonstrates that the increased $w(12k)$ weight leads to a reduction of the saturation magnetization compared to the case of uniform vacancy distribution and produces a good agreement between our model and the experimental data.

The fact that an increased vacancy weight $w(12k)$ leads to an *increase* of T_c and x_c but a *decrease* of M_s appears somewhat counterintuitive at first glance. However, it can be readily explained by the ferrimagnetic order in the hexaferrites. An increased $w(12k)$ weight reduces the number of Fe atoms in the majority (spin-up) sublattices whereas it increases the number of Fe atoms in the minority (spin-down) sublattices. As a result, the difference between the numbers of spin-up and spin-down Fe ions is reduced, leading to a significant reduction of M_s. Note that this explanation does not rely on non-collinear magnetic order caused by the subleading (frustrating) interactions. We will return to this point in the concluding section.

D. Sublattice magnetizations

In addition to the ferrimagnetic order parameter $\boldsymbol{\psi}$ and the total magnetization **m**, we have also calculated how the sublattice magnetizations $\mathbf{m}_l$ [defined in Eq. (6)] depend on the impurity concentration x, the weights w and the temperature T. Figure 9 shows the sublattice magnetizations as functions of temperature at fixed $x = 3.6$

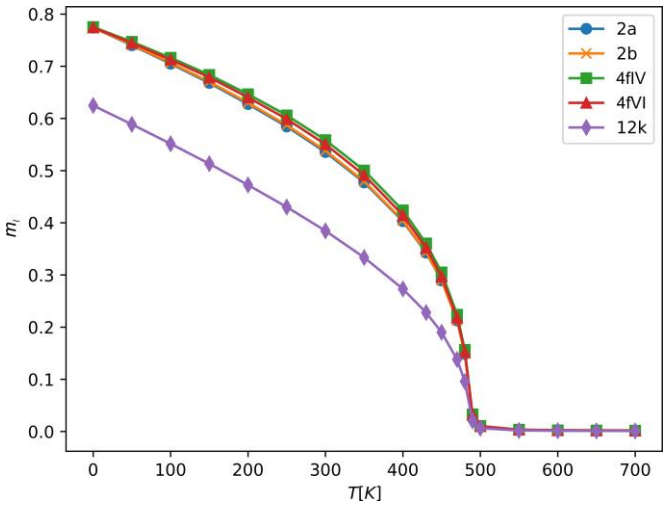

FIG. 9. Sublattice magnetizations m_l vs. temperature T for $x = 3.6$ and $w(12k) = 1.25$. All other weights take the value $2 - w(12k)$.

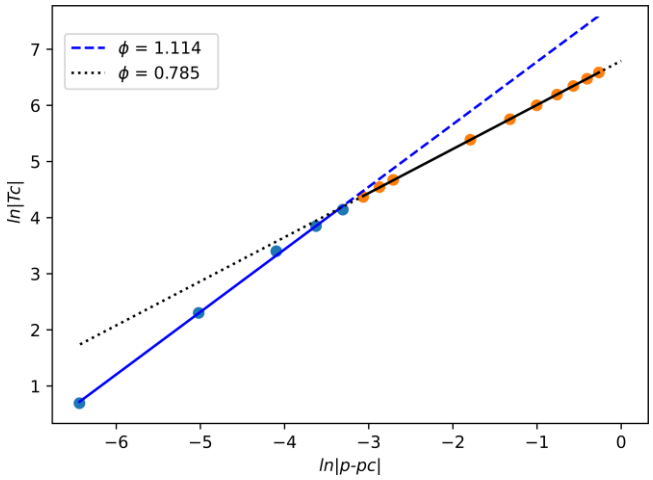

FIG. 10. Ordering temperature T_c vs. distance from the percolation threshold $p_c - p$ for $w(12k) = 1.25$. All other weights take the value $2-w(12k)$. The dashed line is a power- law fit $T_c \sim (p_c - p)^\phi$ of the data points close to x_c. The dotted line is the corresponding fit of the preasymptotic behavior. The statistical errors of the data are smaller than the symbol size.

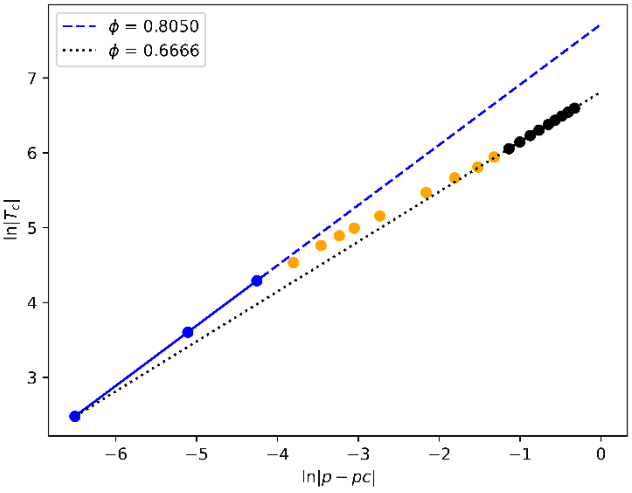

FIG. 11. Ordering temperature T_c vs. distance from the percolation threshold $p_c - p$ for $w(12k) = 1.5$. All other weights take the value $2 - w(12k)$.

and $w(12k) = 1.25$. [All other weights are equal and given by Eq. (3).] As expected, $m_l(12k)$ is significantly lower than all the other sublattice magnetizations because the vacancy concentration in the $12k$ sublattice is higher than those of the other sublattices. In fact, the zero-temperature limit of m_l agrees with the fraction of occupied sites in each sublattice. The differences of the sublattices magnetizations between the other sublattices ($2a$, $2b$, $4f_{IV}$, $4f_{VI}$) are very small. They reflect the differences in the environments of the Fe atoms in the different sublattices.

E. Critical behavior at x_c

Finally, we turn to the critical behavior of the zero-temperature phase transition at x_c. To this end, we analyze the the dependence of T_c on the distance $x - x_c$ from the zero temperature transition. For the case of a uniform vacancy distribution, Khairnar et al. [9] showed that $T_c \sim (x_c - x)^\phi$ with $\phi = 1.12$ in a narrow asymptotic region close to x_c. This value of the crossover exponent ϕ agrees with the predictions of classical percolation theory [25, 26], confirming that transition at x_c is a percolation transition. The pre-asymptotic behavior of T_c further away from x_c still followed a power law in $(x_c - x)$, but with a nonuniversal crossover exponent. Its value was below unity but well above the experimentally observed 2/3.

Here we employ the same analysis for the case of a nonuniform vacancy distribution, specifically for our sequence of systems with increased vacancy weight $w(12k)$ and reduced weights (3) for all other sublattices. We find two different regimes, depending on $w(12k)$.

In the first regime, the zero-temperature transition occurs (as a function of increasing x) before the $12k$ sublattice is completely depleted of Fe atoms. As shown in Fig. 5, this happens for $w(12k) \lessapprox 1.4$. In this regime the behavior of T_c with $x - x_c$ is analogous to the case of uniform dilution: Asymptotically close to x_c, the ordering temperature follows $T_c \sim (x_c - x)^\phi$ with the ϕ value from percolation theory. Further away from x_c, the behavior crosses over to a weaker dependence on x. This is illustrated in Fig. 10 for $w(12k) = 1.25$.

In the second regime, the zero-temperature transition coincides with the complete depletion of the $12k$ sublattice of Fe atoms, as is the case for $w(12k) \gtrapprox 1.4$ (at least in very good approximation). Figure 11 shows the dependence of T_c on $x_c - x$ for $w(12k) = 1.5$ with $x_c = 12/w(12k) = 8$. Clearly, the shape of the phase

boundary $T_c(x)$ differs from the percolation scenario described above, suggesting a different universality class of the zero-temperature critical point.

V. CONCLUSIONS

In summary, motivated by the disagreement between experimental data and theoretical predictions, we have revisited the magnetic properties of diluted hexagonal ferrites, in particular $PbFe_{12-x}Ga_xO_{19}$. We have focused on the effects of an uneven distribution of the nonmagnetic Ga impurities over the five distinct Fe sublattices.

Our ab-initio density-functional calculations have shown that the preferred sublattice for the Ga atoms is the 12*k* sublattice. To include this preference in the Monte-Carlo simulations, we have created model impurity distributions with increased vacancy probability in the 12k sublattice and correspondingly reduced probabilities in all other sublattices. These probabilities are parameterized by weights w such that the vacancy probability in sublattice Y is given by $w(Y)\,p$ with $p = x/12$ the overall vacancy probability.

For appropriately chosen sublattice weights [$w(12k) \approx 1.2$ to 1.3 and the other w correspondingly reduced], our Monte Carlo results for the phase boundary $T_c(x)$ and the low-temperature saturation magnetization M_s are in excellent agreement with the experimental data of Refs. [5–7]. This indicates that the uneven distribution of the Ga impurities is the main reason for the discrepancies between the measurements and previous theoretical work in the literature. Notably, the uneven Ga distribution explains why the experimental saturation magnetization drops rapidly with increasing x whereas the critical temperature T_c decreases much more slowly.

We have also studied the critical behavior of the zero-temperature phase transition at the critical Ga concentration x_c. If this transition happens before any of the sublattices becomes completely depleted of Fe, the critical behavior of T_c follows the predictions of percolation theory. For a more unequal Ga distribution (larger weight $w(12k) \gtrapprox 1.4$), the zero-temperature transition coincides with the emptying of the 12*k* sublattice. This leads to a different critical behavior of $T_c(x)$.

Our results suggest that the agreement between the experimental T_c data and the striking 2/3 power-law behavior of the phase boundary $T_c(x)$ put forward in Ref. [5] is actually "accidental." It appears to be the result of the particular Ga weights rather than a fundamental principle. In fact, the data in Fig. 7 suggest that the 2/3 power law may not accurately describe the data close to x_c. Testing this predictions requires additional experiments at Ga concentrations close to x_c.

The Ga distributions employed in our simulations should be considered simple models rather than a quantitatively accurate description of the real materials. For example, we do not include possible dependencies of the weights w on the concentration x, and we neglect any correlations between neighboring impurities. Extracting a more detailed description of the Ga distribution from our Monte Carlo simulations requires additional experimental input beyond T_c and M_s. In particular, fully disentangling the Ga concentrations in all five sublattices would require the measurement of sublattice magnetization curves (or equivalent local information) over the full x range. To the best of our knowledge, such experimental data are not yet available.

Our present simulations do not include any of the subleading exchange interactions that frustrate the ferrimagnetic order. As a consequence, the magnetic order remains collinear over the entire x range. Simulations performed in Ref. [9] showed that subleading frustrating interactions and the resulting non-collinear order lead to a reduction in T_c. This implies that the frustrating interactions (by themselves) cannot explain the disagreement between the experiments and previous theoretical work. Even though our results demonstrate that non-collinear order is not the main reason for the rapid drop of the saturation magnetization M_s with x, the frustrating interactions and the resulting non-collinear order likely become important at larger x close to the zero-temperature transition.

We hope that our study will encourage further experimental and theoretical work that helps resolving the open questions about the behavior of $PbFe_{12-x}Ga_xO_{19}$ and other diluted hexaferrites.

ACKNOWLEDGMENTS

This work has been supported in part by the National Science Foundation under Grant Nos. DMR-1828489 and OAC-1919789. The simulations were performed on the Pegasus and Foundry clusters at Missouri S&T.

[1] R. C. Pullar, Progress in Materials Science **57**, 1191 (2012).

[2] R. C. Pullar, in *Mesoscopic Phenomena in Multifunctional Materials: Synthesis, Characterization, Modeling and Applications*, edited by A. Saxena and A. Planes (Springer, Berlin, 2014) pp. 159–200.

[3] S. E. Rowley, Y.-S. Chai, S.-P. Shen, Y. Sun, A. T. Jones, B. E. Watts, and J. F. Scott, Scientific Reports **6**, 25724 (2016).

[4] S.-P. Shen, J.-C. Wu, J.-D. Song, X.-F. Sun, Y.-F. Yang, Y.-S. Chai, D.-S. Shang, S.-G. Wang, J. F. Scott, and Y. Sun, Nature Communications **7**, 10569 (2016).

[5] S. E. Rowley, T. Vojta, A. T. Jones, W. Guo, J. Oliveira, F. D. Morrison, N. Lindfield, E. Baggio Saitovitch, B. E. Watts, and J. F. Scott, Phys. Rev. B **96**, 020407 (2017).

[6] M. Marysko, Z. Frait, and S. Krupicka, J. Phys. IV France **07**, C1 (1997).

[7] G. Albanese, F. Leccabue, B. E. Watts, and S. D´ıaz-Castañón, J. Mat. Sci **37**, 3759 (2002).

[8] E. Lieb and D. Mattis, Journal of Mathematical Physics **3**, 749 (1962).

[9] G. Khairnar, C. Lerch, and T. Vojta, Eur. Phys. J. B **94**, 43 (2021).

[10] G. Albanese, M. Carbucicchio, and A. Deriu, Nuovo Cimento **15**, 147 (1973).

[11] G. Albanese, M. Carbucicchio, and A. Deriu, Physica Status Solidi (a) **23**, 351 (1974).

[12] G. K. Thompson and B. J. Evans, J. Appl. Phys. **75**, 6643 (1994).

[13] V. Dixit, C. N. Nandadasa, S.-G. Kim, S. Kim, J. Park, and Y.-K. Hong, J. Appl. Phys. **118**, 203908 (2015).

[14] P. Nov´ak and J. Rusz, Phys. Rev. B **71**, 184433 (2005).

[15] C. Wu, Z. Yu, K. Sun, J. Nie, R. Guo, H. Liu, X. Jiang, and Z. Lan, Scientific Reports **6**, 36200 (2016).

[16] C. Tejera-Centeno, S. Gallego, and J. Cerd´a, Scientific Reports **11**, 1964 (2021).

[17] R. D. Shannon, Acta Crystallographica Section A **32**, 751 (1976).

[18] U. Wolff, Phys. Rev. Lett. **62**, 361 (1989).

[19] N. Metropolis, A. W. Rosenbluth, M. N. Rosenbluth, A. H. Teller, and E. Teller, J. Chem. Phys. **21**, 1087 (1953).

[20] H. G. Ballesteros, L. A. Fern´andez, V. Mart´ın-Mayor, A. Muñoz Sudupe, G. Parisi, and J. J. Ruiz-Lorenzo, Phys. Rev. B **58**, 2740 (1998).

[21] T. Vojta and R. Sknepnek, Phys. Rev. B **74**, 094415 (2006).

[22] Q. Zhu, X. Wan, R. Narayanan, J. A. Hoyos, and T. Vojta, Phys. Rev. B **91**, 224201 (2015).

[23] K. Binder, Phys. Rev. Lett. **47**, 693 (1981).

[24] M. E. J. Newman and R. M. Ziff, Phys. Rev. E **64**, 016706 (2001).

[25] D. Stauffer and A. Aharony, *Introduction to Percolation Theory* (CRC Press, Boca Raton, 1991).

[26] A. Coniglio, Phys. Rev. Lett. **46**, 250 (1981).

Magnetic Properties of Diluted Hexaferrites - Reflection

Logan Sowadski

Throughout my project investigating the magnetic properties of diluted hexaferrites, I have gained a strong understanding of the process of research in the field of computational physics. Our research question arose from inconsistencies between theoretical predictions and experimental observations on the magnetic behavior of the hexaferrite as it became increasingly more diluted. We try to understand the cause for this discrepancy and project the material's behavior as it becomes increasingly more diluted through computer simulations and data analysis. With my advisor Dr. Vojta, I was guided through this research process and now have an understanding of the process of researching a problem or question using computation resources.

This was my first experience doing research and it required me to expand my knowledge of modern physics and modern methods of solving problems. I had to make strong use of informational resources to learn more about these projects as a lot of the information is in publisher archives. Through searching archives such as arXiv, SpringerLink, and the APS's, I was able to easily search for papers and information that would assist me in designing my code and performing data analysis on the system.

Our experiment was done through computational simulations. The experimental set up for these relies a lot on how we are wanting to model our system. I learned why you may want to design systems in particular ways and why we chose specifically to look at our system through what is known as a 'Heisenberg' model. Our experimental setup as well relies a lot on the infrastructure we set up in our program in order to ensure we could get as accurate of a calculation as possible while minimizing the run time of our simulation. This required me to learn how to make use of parallel computing to spread out the work across individual nodes to

make the computations as efficient as possible.

During the entirety of the project, Dr. Vojta took a major role in being the one to introduce me to new material and giving me a basic understanding to build on myself through supplemental resources. Doing this throughout the entire duration of the project made the results and the actual physics of the project very easy to digest. In a computational environment where we are mostly working with numbers and code, being able to interpret the physical meaning of results is difficult. The long process of getting everything ready for publication helped me understand the information as well. We were very careful in the writing process to present all of our data while making the material digestible for a reader. This required me to have a very deep knowledge not only of my work but the papers that have led up to mine.